# Controlling Population Size and Mutation Strength by Meta-ES under Fitness Noise

Hans-Georg Beyer
Research Center PPE
Vorarlberg University of Applied Sciences
Dornbirn, Austria
Hans-Georg.Beyer@fhv.at

Michael Hellwig
Research Center PPE
Vorarlberg University of Applied Sciences
Dornbirn, Austria
Michael.Hellwig@fhv.at

## ABSTRACT

This paper investigates strategy parameter control by Meta-ES using the noisy sphere model. The fitness noise considered is normally distributed with constant noise variance. An asymptotical analysis concerning the mutation strength and the population size is presented. It allows for the prediction of the Meta-ES dynamics. An expression describing the asymptotical growth of the normalized mutation strength is calculated. Finally, the theoretical results are evaluated empirically.

## Categories and Subject Descriptors

I.2.8 [**Problem Solving, Control Methods, and Search**]: Control theory

## Keywords

Adaptation, Evolution Strategies, Meta-ES, Mutation Strength, Population Size, Sphere Model, Fitness Noise

## 1. INTRODUCTION

In the field of Evolution Strategies (ESs) hierarchical organized ESs also referred to as Meta-ESs have proven themselves useful for learning the optimal strategy parameters depending on the underlying optimization problem. According to Rechenberg [8], a Meta-ES is formally defined by generalizing the ES bracket notation to

$$[\mu'/\rho', \lambda'(\mu/\rho, \lambda)^\gamma]\,. \tag{1}$$

In (1), $\lambda'$ offspring populations conducting $(\mu/\rho, \lambda)$-ESs run parallelly over a number of $\gamma$ generations. Each of these ESs is realized in isolation from the others and holds different initial strategy parameters. Selection on the upper level then chooses those $\mu'$ populations for recombination which are identified to have the best strategy parameters w.r.t. a previously defined fitness criterion. Proceeding this way the Meta-ES is expected to direct the strategy parameters to optimality.


*FOGA'13,* January 16-20, 2013, Adelaide, Australia.


Systematic investigations on the dynamics of Meta-ES are still rare. First results were obtained by Herdy [7] who investigated Meta-ES on a set of test functions. Furthermore he was the first to provide evidence that Meta-ES can direct the inner ES to optimal performance. After some years without theoretical research on the topic Arnold [3] presented an analysis of the mutation strength adaptation by $[1, 2(\mu/\mu_I, \lambda)^\gamma]$-Meta-ES on the class of ridge functions. While his analysis concerned a wide class of ridge functions, however, it excluded the sharp ridge function. The latter has been investigated by Beyer and Hellwig in [6]. In [5], Beyer et al. also analyzed the performance of the $[1, 2(\mu/\mu_I, \lambda)^\gamma]$-Meta-ES on the sphere model $F(\mathbf{y}) = f(\|\mathbf{y} - \hat{\mathbf{y}}\|)$ considering a simple Meta-ES which controls the mutation strength and the parental population size to (near) optimality.

This paper is going to pick up on that analysis of Meta-ES on the sphere model. It extends the investigated Meta-ES algorithm and considers additionally the sphere model with fitness noise. The paper aims at learning about the ability of the specific Meta-ES to deal with the noisy optimization problem. A Meta-ES variant which simultaneously controls two strategy parameters is considered. Carrying out the theoretical analysis we expect to develop a more thorough understanding of the interactions between the different dynamics. In the following sections we analyze the behavior of Meta-ESs in the fitness environment defined by the N-dimensional sphere model under the influence of fitness noise with constant variance, i.e., *constant noise* for short

$$\tilde{F}(\mathbf{y}) = \sum_{j=1}^{N} y_j^2 + \mathcal{N}(0, \sigma_\epsilon^2). \tag{2}$$

The constant fitness noise in (2) is modeled by means of an additive normally distributed term with mean zero and constant standard deviation $\sigma_\epsilon$. Note, that $\sigma_\epsilon$ will be referred to as the noise strength. Fitness noise affects the selection mechanism of the Meta-ES algorithm. That is, the measured fitness $\tilde{F}(\mathbf{y})$ of a candidate solution $\mathbf{y}$ will not longer comply with the ideal fitness $F(\mathbf{y})$ but it is normally distributed with mean $F(\mathbf{y})$ and standard deviation $\sigma_\epsilon$. As a consequence this may lead to the selection of inferior solutions based on their measured fitness while superior solutions are eliminated.
We will particularly focus on the control of the mutation strength $\sigma$ as well as the parental population size $\mu$. Considering constant fitness noise throughout the search space, it is not possible to determine the exact location of the optimizer with a regular ES on the spherical fitness environment, see [1]. After a number of generations the distance to the optimizer will fluctuate around a nonzero mean which increases with increasing noise strength. This residual distance can only be decreased by increasing the population size of the ES. As we will see, considering the idealized mean value

dynamics, at first priority the Meta-ES will increase the population size up to a predefined maximal value and subsequently the strategy constantly decreases the mutation strength while keeping the population size constant at its maximal value. Consequently this leads to a permanent approach to the final residual distance.

The paper is organized as follows: In Sec. 2 we present a simple $[1, 4(\mu/\mu_I, \lambda)^\gamma]$-Meta-ES which is intended to control $\sigma$ and $\mu$ at the same time. Sec. 3 then builds the basis of our theoretical analysis by describing the dynamics of the inner ES and providing useful approximations. Subsequently in Sec. 4 we investigate the dynamics of the population sizes $\mu$ and $\lambda$ with fixed truncation ratio $\nu$. Afterwards, the theoretical analysis of the $\sigma$-dynamics follow in Sec. 5. A comparison with real Meta-ES runs is presented in Sec. 6. Finally, Sec. 7 provides a summary of the results and gives an outlook into future research opportunities.

## 2. THE [1, 4]-META-ES ALGORITHM

In this section we introduce the $[1, 4(\mu/\mu_I, \lambda)^\gamma]$-Meta-ES algorithm. Using a deterministic adaptation rule the outer ES controls the population sizes $\mu$, and $\lambda$ as well as the mutation strength $\sigma$. The outer strategy is presented in Fig. 1.

| $[1, 4(\mu/\mu_I, \lambda)^\gamma]$-ES | Line |
|---|---|
| Initialize($\mathbf{y_p}, \sigma_p, \alpha, \beta, \mu_p, \nu, \gamma_p, N$); | 1 |
| $d \leftarrow \gamma_p \mu_p$; | 2 |
| $t \leftarrow 0$; | 3 |
| Repeat | 4 |
| $\tilde{\sigma}_1 \leftarrow \sigma_p \alpha$; $\tilde{\sigma}_2 \leftarrow \sigma_p / \alpha$; | 5 |
| Select case $\mu_p$ | 6 |
| case $\mu_p = 1$: $\tilde{\mu}_1 \leftarrow \mu_p \beta$; $\tilde{\mu}_2 \leftarrow 1$; | 7 |
| case $\mu_p = d$: $\tilde{\mu}_1 \leftarrow d$; $\tilde{\mu}_2 \leftarrow \mu_p / \beta$; | 8 |
| case Else: $\tilde{\mu}_1 \leftarrow \mu_p \beta$; $\tilde{\mu}_2 \leftarrow \mu_p / \beta$; | 9 |
| End Select | 10 |
| $\tilde{\lambda}_1 \leftarrow \tilde{\mu}_1 / \nu$; $\tilde{\lambda}_2 \leftarrow \tilde{\mu}_2 / \nu$; | 11 |
| $\tilde{\gamma}_1 \leftarrow d / \tilde{\mu}_1$; $\tilde{\gamma}_2 \leftarrow d / \tilde{\mu}_2$; | 12 |
| $[\tilde{\mathbf{y}}_\mathbf{1}, \tilde{F}_1, \sigma_1, \mu_1] \leftarrow \mathrm{ES}(\tilde{\mu}_1, \tilde{\lambda}_1, \tilde{\gamma}_1, \tilde{\sigma}_1, \mathbf{y_p})$; | 13 |
| $[\tilde{\mathbf{y}}_\mathbf{2}, \tilde{F}_2, \sigma_2, \mu_2] \leftarrow \mathrm{ES}(\tilde{\mu}_1, \tilde{\lambda}_1, \tilde{\gamma}_1, \tilde{\sigma}_2, \mathbf{y_p})$; | 14 |
| $[\tilde{\mathbf{y}}_\mathbf{3}, \tilde{F}_3, \sigma_3, \mu_3] \leftarrow \mathrm{ES}(\tilde{\mu}_2, \tilde{\lambda}_2, \tilde{\gamma}_2, \tilde{\sigma}_1, \mathbf{y_p})$; | 15 |
| $[\tilde{\mathbf{y}}_\mathbf{4}, \tilde{F}_4, \sigma_4, \mu_4] \leftarrow \mathrm{ES}(\tilde{\mu}_2, \tilde{\lambda}_2, \tilde{\gamma}_2, \tilde{\sigma}_2, \mathbf{y_p})$; | 16 |
| $\mathbf{y_p} \leftarrow \tilde{\mathbf{y}}_{\mathbf{1;4}}$; | 17 |
| $\sigma_p \leftarrow \sigma_{1;4}$; | 18 |
| $\mu_p \leftarrow \mu_{1;4}$; | 19 |
| $t \leftarrow t + 1$; | 20 |
| Until(termination condition) | 21 |

**Figure 1: Pseudo code of the [1, 4]-Meta-ES. The Code of the inner ES is displayed in Fig. 2.**

In Line 2 the parameter $d$ is defined as the product of the initial isolation length $\gamma_p$ and the initial population size $\mu_p$. It is used as an upper bound for these two strategy parameters and kept constant. The algorithm is running four competing inner $[(\mu/\mu_I, \lambda)^\gamma]$-ESs which start at the same initial $\mathbf{y_p}$ (parental $\mathbf{y}$) but differ in the choice of the population size and the mutation strength. Two offspring mutation strength parameters $\tilde{\sigma}_1$ and $\tilde{\sigma}_2$ are generated in Line 5 by increasing and decreasing the parental mutation strength $\sigma_p$ by a factor $\alpha$. From Line 6 up to Line 11 we create the new population size parameters. At first two parameters $\tilde{\mu}_1$ and $\tilde{\mu}_2$ are computed by increasing/decreasing the parental $\mu_p$ by a factor $\beta$. If $\mu_p$ has already reached its lower bound, i.e. $\mu_p = 1$, or its upper bound $d$, $\mu_p$ is only modified in one direction, i.e. increased or decreased, respectively, and kept constant for the other parameter. Dividing the new parental population sizes $\tilde{\mu}_j$ by the fixed truncation ratio $\nu$ leads to the corresponding offspring population size parameters $\tilde{\lambda}_1$ and $\tilde{\lambda}_2$.

The isolation length parameters $\tilde{\gamma}_1$ and $\tilde{\gamma}_2$ are defined depending on $\tilde{\mu}_1$ and $\tilde{\mu}_2$ in Line 12, always complying with the condition [1]

$$d = \gamma\mu \quad \Leftrightarrow \quad d/\nu = \lambda\gamma. \tag{3}$$

Identifying $\lambda\gamma$ with the number of function evaluations during a single inner ES run, the way of controlling $\gamma$ in (3) keeps the number of function evaluations over all observed isolation periods equal. Each combination of the two different population sizes $(\tilde{\mu}_j, \tilde{\lambda}_j)$ with corresponding isolation length $\tilde{\gamma}_j$ and the two mutation strength parameters $\tilde{\sigma}_j$ (j=1, 2) serves as strategy parameter set and is held constant within the inner ES. After having evolved over their associated isolation length, each inner ES returns the centroid of its final parental population $\mathbf{y_k}$ and its corresponding fitness value $F_k = F(\mathbf{y_k})$, $k = 1, \ldots, 4$. Finally the selection in the [1, 4]-Meta-ES is performed in Lines 17 to 19 using the standard notation "$m; \lambda'$" indicating the $m$-th best population out of $\lambda'$ populations with respect to the fitness value generated by the respective inner $(\mu/\mu, \lambda)$-ES. That is, the strategy parameters of the best inner population are used as parental parameters in the outer ES.

The termination criterion can be specified as a fixed number of isolation periods $t$, or function evaluations respectively.

| Function: ES($\mu, \lambda, \gamma, \sigma, \mathbf{y}$) | Line |
|---|---|
| $g \leftarrow 1$; | 1 |
| While $g \leq \gamma$ | 2 |
| For $l = 1$ To $\lambda$ | 3 |
| $\tilde{\mathbf{y}}_l \leftarrow \mathbf{y} + \sigma \mathcal{N}_l(0, \mathbf{I})$; | 4 |
| $\tilde{F}_l \leftarrow F(\tilde{\mathbf{y}}_l)$; | 5 |
| End For | 6 |
| $\mathbf{y} \leftarrow \frac{1}{\mu} \sum_{m=1}^{\mu} \tilde{\mathbf{y}}_{m;\lambda}$; | 7 |
| $g \leftarrow g + 1$; | 8 |
| End While | 9 |
| Return $[\mathbf{y}, F(\mathbf{y}), \sigma, \mu]$; | 10 |

**Figure 2: The inner $(\mu/\mu_I, \lambda)^\gamma$-ES**

The inner ES, see Fig. 2, generates a population of $\lambda = \mu/\nu$ offspring by adding a $\sigma$ mutation strength scaled vector of independent, standard normally distributed components to the centroid $\mathbf{y}$ of the parental generation. The $\mu$ best candidates in terms of their function values $\tilde{F}_l$ are chosen out of these $\lambda$ offspring and used to build the new parental centroid $\mathbf{y}$. Proceeding this way over $\gamma$ generations, the inner ES returns the tuple $[\mathbf{y}, F(\mathbf{y}), \sigma, \mu]$.

## 3. THEORETICAL ANALYSIS REGARDING CONSTANT NOISE

In this section we are going to investigate the dynamics of the inner $(\mu/\mu, \lambda)$-ES assuming that the observed fitness is disturbed by a noise term with constant noise strength $\sigma_\epsilon$. Beginning with the distance to the optimizer $R(g)$ in generation $g$ we are interested in finding a prediction of the distance $R^{(g+\gamma)}$ at the end of a single isolation period of $\gamma$ generations. The starting point of the theoretical analysis is the normalized progress rate in the limit of infinite

[1] In order to always obtain integer values for $\mu$, $\lambda$, and $\gamma$, the initial $\mu_p$, $\gamma_p$ and $\beta$, $1/\nu$ are chosen as powers of two.

search space dimensionality

$$\varphi^*(\sigma^*, \sigma_\epsilon^*) = \frac{c_{\mu/\mu,\lambda}\sigma^{*2}}{\sqrt{\sigma^{*2} + \sigma_\epsilon^{*2}}} - \frac{\sigma^{*2}}{2\mu}. \tag{4}$$

The normalized quantities used in Eq. (4) are given by

$$\sigma^* = \sigma\frac{N}{R}, \quad \sigma_\epsilon^* = \sigma_\epsilon\frac{N}{2R^2}, \text{ and } \quad \varphi^* = \varphi\frac{N}{R}. \tag{5}$$

For a precise mathematical derivation of $\varphi^*$ we refer to [2, 1]. The definition of the progress coefficient $c_{\mu/\mu,\lambda}$ can be found in [4]. Note that according to (4) positive progress will only be achieved if the condition

$$\sigma^{*2} + \sigma_\epsilon^{*2} < (2\mu c_{\mu/\mu,\lambda})^2 \tag{6}$$

holds. That directly indicates an upper bound of $2\mu c_{\mu/\mu,\lambda}$ for the normalized mutation strength $\sigma^*$ and the normalized noise strength $\sigma_\epsilon^*$ as well.

Applying the re-normalizations to Eq. (4) and taking into account the $\varphi$ definition

$$\varphi^{(g)} = R^{(g)} - R^{(g+1)} \tag{7}$$

we obtain the difference equation

$$\boxed{R^{(g)} - R^{(g+1)} = \frac{2c_{\mu/\mu,\lambda}R\sigma^2}{\sqrt{4R^2\sigma^2 + {\sigma_\epsilon}^2}} - \frac{N\sigma^2}{2\mu R}.} \tag{8}$$

Equation (8) indicates the expected change in the distance to the optimizer between two consecutive generations.

On the basis of (8) we compute the expected steady state distance $\tilde{R}_\infty(\sigma, \sigma_\epsilon)$. It predicts the residual distance to the optimizer which can be reached by the inner ES if the ES runs for a infinite number of generations given a fixed mutation strength $\sigma$ and constant population sizes $\mu$ and $\lambda$. Solving $0 = \varphi(\sigma, \sigma_\epsilon, \tilde{R}_\infty)$ for $\tilde{R}_\infty$, we obtain

$$\tilde{R}_\infty(\sigma, \sigma_\epsilon) = \sqrt{\frac{N^2\sigma^2 + \sqrt{4\mu^2 c_{\mu/\mu,\lambda}^2 N^2\sigma_\epsilon^2 + N^4\sigma^4}}{8\mu^2 c_{\mu/\mu,\lambda}^2}} \tag{9}$$

$$\tilde{R}_\infty(\sigma, \sigma_\epsilon) = R_\infty(\sigma)\sqrt{\frac{1}{2}\left(1 + \sqrt{1 + \frac{\vartheta^2}{R_\infty(\sigma)^2}}\right)} \tag{10}$$

with noise-to-signal ratio $\vartheta = \frac{\sigma_\epsilon}{\sigma}$ and the noise-free steady state distance

$$R_\infty(\sigma) = \frac{N\sigma}{2\mu c_{\mu/\mu,\lambda}}. \tag{11}$$

Considering small mutation strength sizes, i.e. $\sigma \to 0$, Eq. (9) is becoming

$$\boxed{\hat{R}_\infty = \sqrt{\frac{N\sigma_\epsilon}{4\mu c_{\mu/\mu,\lambda}}}} \tag{12}$$

which is already known as a good approximation of the expected steady state distance $\tilde{R}_\infty$ in the vicinity of small mutation strengths, see [1].

Because we are not able to find a closed analytical solution of the nonlinear difference equation (8) for $R^{(g+1)}$ we search for a good approximation. Approximating (8) is formally done by switching to the continuous time limit and expanding $R(g+1)$ in a Taylor series at $g$. Identifying $R(g+1)$ with $R^{(g+1)}$ and $R(g)$ with $R^{(g)}$ then yields

$$R^{(g+1)} - R^{(g)} = \frac{dR}{dg}1 + \dots . \tag{13}$$

Thus, by applying Eq. (8) one obtains a nonlinear differential equation which approximates the progress dynamics

$$\frac{dR}{dg} = \frac{N\sigma^2}{2\mu R} - \frac{2c_{\mu/\mu,\lambda}R\sigma^2}{\sqrt{4R^2\sigma^2 + {\sigma_\epsilon}^2}}. \tag{14}$$

However, even (14) is rather difficult to be solved. Therefore, we are searching for a linear approximation describing the dynamics towards $\tilde{R}_\infty$. Expanding (14) into a Taylor series about $\tilde{R}_\infty$, we get

$$\frac{dR}{dg} \approx \left(\frac{8c_{\mu/\mu,\lambda}\tilde{R}_\infty^2\sigma^4}{\sqrt{\left(\sigma_\epsilon^2 + 4\tilde{R}_\infty^2\sigma^2\right)^3}} - \frac{N\sigma^2}{2\tilde{R}_\infty^2\mu} - \frac{2c_{\mu/\mu,\lambda}\sigma^2}{\sqrt{\sigma_\epsilon^2 + 4\tilde{R}_\infty^2\sigma^2}}\right)(R - \tilde{R}_\infty) \tag{15}$$

$$= \left(\frac{8c_{\mu/\mu,\lambda}\tilde{R}_\infty^2\sigma^4}{\sqrt{\left(\sigma_\epsilon^2 + 4\tilde{R}_\infty^2\sigma^2\right)^3}} - \frac{N\sigma^2}{2\tilde{R}_\infty^2\mu} - \frac{2c_{\mu/\mu,\lambda}\sigma^2(\sigma_\epsilon^2 + 4\tilde{R}_\infty^2\sigma^2)}{\sqrt{\left(\sigma_\epsilon^2 + 4\tilde{R}_\infty^2\sigma^2\right)^3}}\right)(R - \tilde{R}_\infty) \tag{16}$$

$$= -\left(\frac{N\sigma^2}{2\tilde{R}_\infty^2\mu} + \frac{2c_{\mu/\mu,\lambda}\sigma^2\sigma_\epsilon^2}{(\sigma_\epsilon^2 + 4\tilde{R}_\infty^2\sigma^2)^{\frac{3}{2}}}\right)(R - \tilde{R}_\infty). \tag{17}$$

Inserting Eq. (17) in (13) we finally obtain

$$R^{(g)} - R^{(g+1)} \approx \left(\frac{N\sigma^2}{2\tilde{R}_\infty^2\mu} + \frac{2c_{\mu/\mu,\lambda}\sigma^2\sigma_\epsilon^2}{(\sigma_\epsilon^2 + 4\tilde{R}_\infty^2\sigma^2)^{\frac{3}{2}}}\right)(R^{(g)} - \tilde{R}_\infty) \tag{18}$$

as a linear approximation of the difference equation (8). For reasons of clarity and comprehensibility we define

$$a \coloneqq \frac{N\sigma^2}{2\tilde{R}_\infty^2\mu} \quad \text{and} \quad b \coloneqq \frac{2c_{\mu/\mu,\lambda}\sigma^2\sigma_\epsilon^2}{(\sigma_\epsilon^2 + 4\tilde{R}_\infty^2\sigma^2)^{\frac{3}{2}}}. \tag{19}$$

Thus, Eq. (18) reads

$$R^{(g+1)} = \left(R^{(g)} - \tilde{R}_\infty\right)(1 - (a+b)) + \tilde{R}_\infty. \tag{20}$$

Computing

$$R^{(g+2)} = \left(R^{(g+1)} - \tilde{R}_\infty\right)(1 - (a+b)) + \tilde{R}_\infty \tag{21}$$

$$= \left(R^{(g)} - \tilde{R}_\infty\right)(1 - (a+b))^2 + \tilde{R}_\infty \tag{22}$$

and continuing this way yields the following equation for the expected distance $R^{(g+\gamma)}$ after one isolation period of $\gamma$ generations

$$\boxed{R^{(g+\gamma)} = \left(R^{(g)} - \tilde{R}_\infty\right)(1 - (a+b))^\gamma + \tilde{R}_\infty.} \tag{23}$$

Assuming that the sum $a + b$ is sufficiently small one can apply the approximation

$$(1 - x)^k \approx 1 - kx \quad \forall x \text{ with } |x| \ll 1. \tag{24}$$

The assumption $a + b \approx 0$ is valid considering sufficiently small mutation sizes $\sigma$, see also (19) for $\sigma \to 0$. Using (24) we obtain an even simpler approximation for the distance to the optimizer after a single inner ES isolation period

$$\boxed{R^{(g+\gamma)} = R^{(g)}(1 - (a+b)\gamma) + \tilde{R}_\infty(a+b)\gamma.} \tag{25}$$

In order to confirm the good compliance between the original Meta-ES dynamics resulting from Eq. (8) and their approximations, see Eq. (23) and Eq. (25), we check the iteratively generated dynamics against each other. The iteration proceeds the following way: Four pairs of strategy parameters are computed from the initial parameters. These are $(\beta\mu, \alpha\sigma)$, $(\beta\mu, \sigma/\alpha)$, $(\mu/\beta, \alpha\sigma)$, and $(\mu/\beta, \sigma/\alpha)$. For each combination of strategy parameters the theoretical equations are iterated over a single isolation period. The length of the isolation period depends on the chosen population size, i.e. it is $\gamma = d/(\beta\mu)$ or $\gamma = (d\beta)/\mu$ respectively. The best of the four independent runs by means of the generated fitness value is selected.

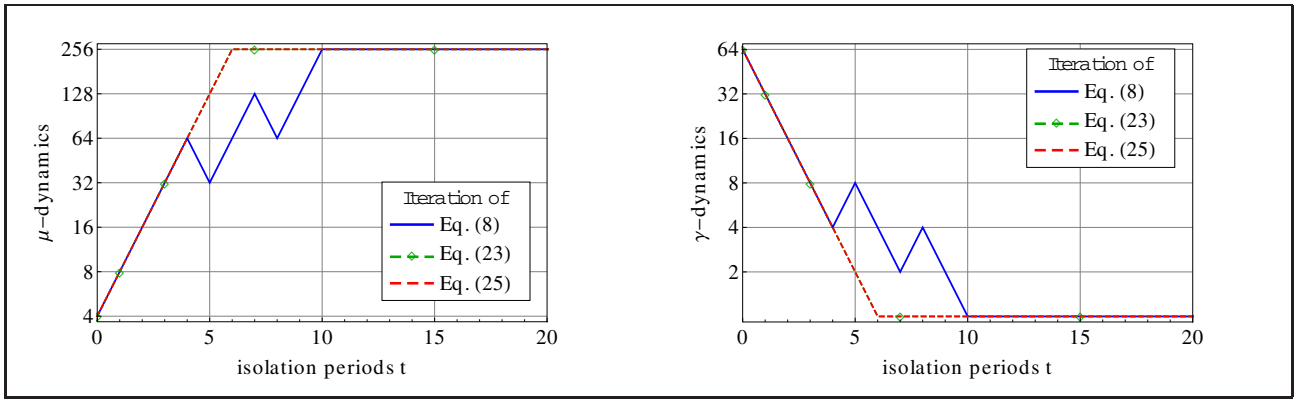


**Figure 3: Illustration of the iteratively computed $\mu$- and $\gamma$-dynamics resulting from Eq. (8) and from its approximations in Eq. (23) and Eq. (25), respectively. To point out the slight differences only the results of the first 20 of 1000 isolation periods are presented.**

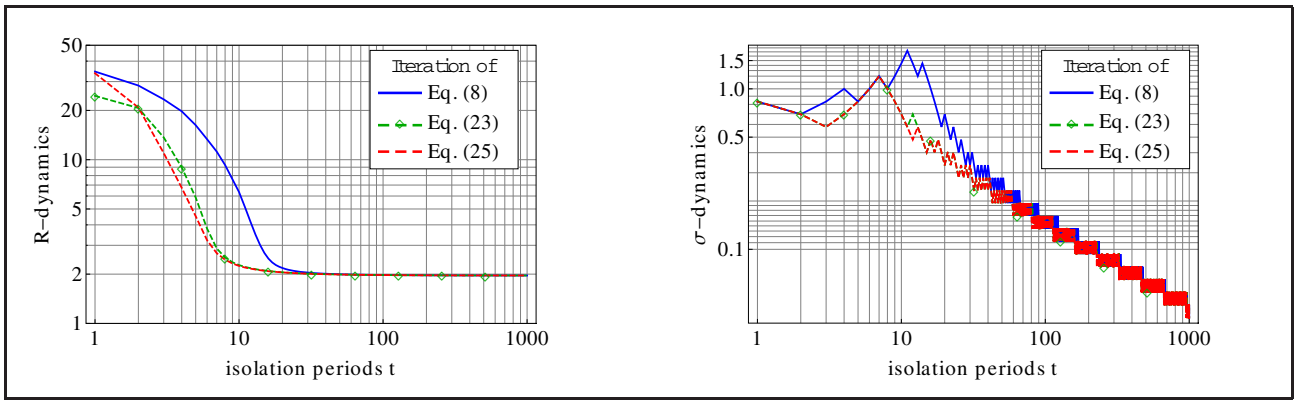


**Figure 4: On the lhs the comparison of the distance $R$ to the optimizer between the iterative results of Eq. (8) and its approximations in Eq. (23) and Eq. (25) is depicted per isolation period, or per $d/\nu = 1024$ function evaluations respectively. The figure on the rhs shows the corresponding mutation strength $\sigma$.**

Its strategy parameters as well as its generated distance $R$ are used as initial strategy parameters of the next iteration step. All results are computed from the same initial values. Figures 3 and 4 display the dynamics. We have chosen a search space dimensionality of $N = 1000$. The initial mutation strength is $\sigma_p = 1$ and the constant noise strength is set to $\sigma_\epsilon = 5$. The initial population sizes are $\mu_p = 4$ and $\lambda_p = 16$, respectively. This is due to the truncation ratio of $\nu = 1/4$. $\gamma_p = 64$ is the initial isolation length. The adjustment parameters are $\alpha = 1.2$ and $\beta = 2$.

In Fig. 3 we present the $\mu$-dynamics in the graph on the lhs and the $\gamma$-dynamics on the rhs. The strategy increases the population size $\mu$ up to its initially defined maximal value $d = 256$. Consequently by construction the corresponding $\gamma$-dynamics show the converse behavior. That is, the isolation length of the inner ES is reduced to 1 by the selection mechanism of the outer ES. The $\mu$-dynamics as well as the $\gamma$-dynamics of the approximations, (23) and (25), perfectly match while they differ slightly from the dynamics of Eq. (8) which is represented by the solid blue line. But these differences can only be observed during the first few isolation periods. All three dynamics overlap after each has finally reached its maximal population size, and minimal isolation length respectively, and remain in this state until the algorithm terminates.

The $R$-dynamics as well as the $\sigma$-dynamics are illustrated in Fig. 4. Again we compare the iteratively computed results of equations (8), (23), and (25). In both cases we notice a similar pattern of the original dynamics and its approximations. After a couple of isolation periods the dynamics almost match. On the rhs the Meta-ES reduces the mutation strength. During the decline the $\sigma$-dynamics show an oscillating behavior. Note that this oscillation phases grow with decreasing $\sigma$. While the oscillations slow down the decrease of the mutation strength, the Meta-ES gradually reduces $\sigma$ and by implication $\sigma^*$, too. A more detailed investigation of this oscillation behavior will be provided in Sec. 5.

Taking a look at the distance $R$ to the optimizer on the lhs of Fig. 4 we observe the dynamics approaching the residual steady state distance $\tilde{R}_\infty$. In fact, since the $\sigma$-dynamics converge to zero the $R$-dynamics approach the approximated steady state distance $\hat{R}_\infty = 1.961$, see Eq. (12).

The good agreement between the dynamics resulting from Eq. (8) and the dynamics iterating its approximations justifies the use of the approximations in the further theoretical investigation of the Meta-ES.

# 4. THE POPULATION SIZE DYNAMICS

This section focuses on the $\mu$-dynamics of the Meta-ES. Since all iterations in the previous section show the strategy's behavior to increase the parental population size $\mu$ to its maximum we are interested in a theoretical analysis. Note that in our considerations $d \coloneqq \mu\gamma$ is defined as the upper bound of the parameter $\mu$, or $\gamma$ respectively.

In the first step we assume a noise free fitness environment ($\sigma_\epsilon = 0$) throughout Sec. 4.1. Afterwards in Sec. 4.2 we include fitness noise into our considerations. In the noise-free case the results from Sec. 3 allow for a rather simple examination of the strategy's population adaptation behavior. Of course, the investigations assuming a noisy fitness landscape are more complicated.

## 4.1 Noise-free Fitness Environment

Since the approximation (25) corresponds well with Eq. (8) and its application simplifies the analysis considerably, we will use (25) as the starting point of the following investigations. Assuming $\sigma^*_\epsilon = 0$, Eq. (25) transforms into

$$R^{(g+\gamma)} = R^{(g)}\,(1 - a\gamma) + \tilde{R}_\infty a\gamma. \tag{26}$$

With $\tilde{R}_\infty(\sigma, 0) = \dfrac{N\sigma}{2\mu c_{\mu/\mu,\lambda}}$, see Eq. (9), and $a = \dfrac{2\mu c^2_{\mu/\mu,\lambda}}{N}$ this yields

$$R^{(g+\gamma)} = R^{(g)}\left(1 - \frac{2c^2_{\mu/\mu,\lambda}}{N}d\right) + c_{\mu/\mu,\lambda}\sigma\gamma. \tag{27}$$

The first addend does no longer depend on either the population size parameter $\mu$[2] or on the mutation strength parameter. This simplifies the following calculations significantly.

After each isolation period the outer ES computes two new parental population sizes $\mu$ by increasing and decreasing the parental population size of the best inner strategy by the parameter $\beta > 1$. In the same manner the algorithm builds two new mutation strengths $\sigma$ by varying the mutation strength of the best inner strategy by the parameter $\alpha$. Thus we obtain the four new strategy parameters which will establish the next four inner ESs

$$\mu_+ \coloneqq \mu\beta \quad \text{and} \quad \mu_- \coloneqq \mu/\beta, \tag{28}$$

as well as

$$\sigma_+ \coloneqq \sigma\alpha \quad \text{and} \quad \sigma_- \coloneqq \sigma/\alpha. \tag{29}$$

Note that $\mu_\pm$, and $\sigma_\pm$ correspond to $\tilde{\mu}_1$ and $\tilde{\mu}_2$, and $\tilde{\sigma}_1$ and $\tilde{\sigma}_2$ respectively, which have been mentioned in Sec. 2.

In this section we apply the following simplification for the progress coefficients

$$c_{\mu/\mu,\lambda} \approx c_{\mu_+/\mu_+,\lambda_+} \approx c_{\mu_-/\mu_-,\lambda_-}. \tag{30}$$

This assumption is valid because in the asymptotic limit case the progress coefficient $c_{\mu/\mu,\lambda}$ only depends on the truncation ratio $\nu = \mu/\lambda$, see also [4].

In the following we identify $R^{(g+\gamma)}_{+-}$ with the expected distance realized by the inner ES that operates with $\mu_+$ and $\sigma_-$ over a single isolation period. The expected distances of the three other inner strategies $R^{(g+\gamma)}_{++}$, $R^{(g+\gamma)}_{-+}$, and $R^{(g+\gamma)}_{--}$ are defined analogously. Consequently using Eq. (27) we get

$$R^{(g+\gamma)}_{++} = R^{(g)}\left(1 - \frac{2c^2_{\mu/\mu,\lambda}}{N}d\right) + c_{\mu/\mu,\lambda}\sigma\alpha\frac{\gamma}{\beta}, \tag{31}$$

$$R^{(g+\gamma)}_{+-} = R^{(g)}\left(1 - \frac{2c^2_{\mu/\mu,\lambda}}{N}d\right) + c_{\mu/\mu,\lambda}\frac{\sigma}{\alpha}\frac{\gamma}{\beta}, \tag{32}$$

$$R^{(g+\gamma)}_{-+} = R^{(g)}\left(1 - \frac{2c^2_{\mu/\mu,\lambda}}{N}d\right) + c_{\mu/\mu,\lambda}\sigma\alpha\gamma\beta, \tag{33}$$

$$R^{(g+\gamma)}_{--} = R^{(g)}\left(1 - \frac{2c^2_{\mu/\mu,\lambda}}{N}d\right) + c_{\mu/\mu,\lambda}\frac{\sigma}{\alpha}\gamma\beta. \tag{34}$$

The algorithm chooses the strategy parameter of the inner ES which generates the smallest distance $R$ to the optimizer. That is, by comparing two expected distances the sign of their difference indicates which strategy is preferred by the Meta-ES. Thus in order to compare all four inner strategies against each other we have to consider six different cases.

At first we examine the four cases which differ in the population parameter $\mu$. Remembering the condition $1 < \alpha < \beta$ we get

$$R^{(g+\gamma)}_{++} - R^{(g+\gamma)}_{-+} = c_{\mu/\mu,\lambda}\sigma\gamma\frac{(\alpha - \alpha\beta^2)}{\beta} < 0, \tag{35}$$

$$R^{(g+\gamma)}_{++} - R^{(g+\gamma)}_{--} = c_{\mu/\mu,\lambda}\sigma\gamma\frac{(\alpha^2 - \beta^2)}{\alpha\beta} < 0, \tag{36}$$

$$R^{(g+\gamma)}_{+-} - R^{(g+\gamma)}_{-+} = c_{\mu/\mu,\lambda}\sigma\gamma\left(\frac{1}{\alpha\beta} - \alpha\beta\right) < 0, \tag{37}$$

$$R^{(g+\gamma)}_{+-} - R^{(g+\gamma)}_{--} = c_{\mu/\mu,\lambda}\sigma\gamma\frac{(\alpha - \alpha\beta^2)}{\alpha^2\beta} < 0. \tag{38}$$

It can be observed that the Meta-ES favors the inner ESs with the higher population size $\mu$. Thus the Meta-ES is expected to permanently increase the parental population size $\mu$ after each isolation period of $\gamma$ generations until finally the upper bound $d$ is reached. Consequently the strategy decreases the isolation length $\gamma$ down to 1. Now we consider the two remaining cases

$$R^{(g+\gamma)}_{++} - R^{(g+\gamma)}_{+-} = c_{\mu/\mu,\lambda}\sigma\gamma\frac{(\alpha^2\beta - \beta)}{\alpha\beta^2} > 0, \tag{39}$$

$$R^{(g+\gamma)}_{-+} - R^{(g+\gamma)}_{--} = c_{\mu/\mu,\lambda}\sigma\gamma\frac{(\alpha^2\beta - \beta)}{\alpha} > 0. \tag{40}$$

We observe that the Meta-ES prefers the strategies which operate with the decreased mutation strength $\sigma_-$.

Thus $R^{(g+\gamma)}_{+-}$ dominates the other three expected distances. That is, the Meta-ES is to be expected to choose the inner strategy which increases the population size $\mu$ and simultaneously decreases the mutation strength $\sigma$. That is, in the absence of fitness noise the $\mu$- and $\sigma$-dynamics can be characterized by

$$\mu^{(g+\gamma)} = \mu^{(g)}\beta \quad \text{and} \tag{41}$$

$$\sigma^{(g+\gamma)} = \sigma^{(g)}/\alpha \tag{42}$$

until the upper bound $d$ of the population size parameter is reached. After that, the population size $\mu$ remains in its maximum while the mutation strength $\sigma$ is decreased further on. An illustration of the $\mu$ and $\sigma$ dynamics in the noise-free fitness case is given in Fig. 5. The dynamics are generated by iteration of Eq. (25). Except for the noise strength ($\sigma_\epsilon = 0$) all initial parameters agree with their choices in Sec. 3. That is, we chose $N = 1000$, $\mu_p = 4$, $\nu = 1/4$, $\lambda_p = 16$, $\beta = 2$, $\gamma_p = 64$, $\sigma_p = 1$ and $\alpha = 1.2$.

According to our predictions, see (41) and (42), the population size $\mu$ is increased until it reaches its maximal value $d$. Furthermore

[2] Assuming a sufficiently large population size such that $c_{\mu/\mu,\lambda}$ depends only on the truncation ratio $\mu/\lambda$.

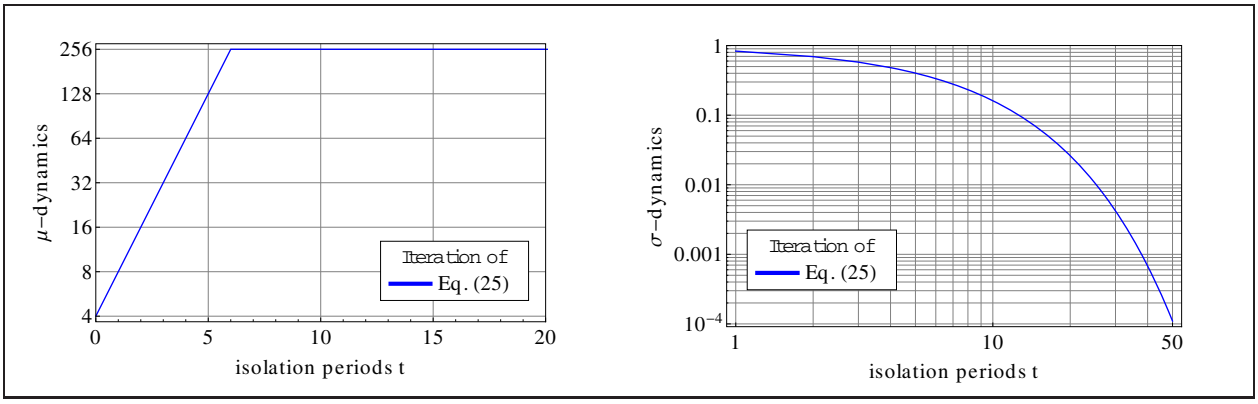


**Figure 5: On the left hand side the $\mu$-dynamic resulting from the iteration of Eq. (25) is shown. The noise strength is $\sigma_\epsilon = 0$. The right hand side presents the respective $\sigma$ dynamics. The initial population size is $\mu = 4$ and the initial isolation length is $\gamma = 64$, i.e. their upper bound is set to $d = 256$.**

the Meta-ES steadily decreases the mutation strength $\sigma$ over the observed isolation periods.

## 4.2 $\mu$-Dynamics Considering Fitness Noise

The next step includes fitness noise into our considerations. We already know that the choice of a higher population size allows for a lower residual distance in standard ESs [1]. That is why, in the presence of fitness noise with constant noise strength $\sigma_\epsilon$, we conclude that the Meta-ES increases the population size $\mu$ to its maximum $d$ just like in the noise-free case. Operating at maximal population size, the isolation inside the algorithm only proceeds over one generation, i.e. $\gamma = 1$. Therefore, it is possible to analyze the $\mu$ dynamics easily. Moreover, considering sufficiently small $\sigma$, the change in the mutation strength between two consecutive isolation periods is neglectable. Using Eq. (4) and (5) we get

$$R^{(g+1)} = R^{(g)} - \varphi^* \frac{R^{(g)}}{N}. \tag{43}$$

Remembering (28) and ignoring the $\sigma$ adaptation at this point, we write $R_+^{(g+1)}$ and $R_-^{(g+1)}$ for the expected distance which is realized by the inner ES that operates with $\mu_+$ and $\mu_-$, respectively. Hence the two expected distances at the end of the isolation period are

$$R_+^{(g+1)} = R^{(g)} - \left( \frac{c_{\mu/\mu,\lambda}\sigma^{*2}}{\sqrt{\sigma_\epsilon^{*2} + \sigma^{*2}}} - \frac{\sigma^{*2}}{2\beta\mu} \right) \frac{R^{(g)}}{N}, \tag{44}$$

$$R_-^{(g+1)} = R^{(g)} - \left( \frac{c_{\mu/\mu,\lambda}\sigma^{*2}}{\sqrt{\sigma_\epsilon^{*2} + \sigma^{*2}}} - \frac{\beta\sigma^{*2}}{2\mu} \right) \frac{R^{(g)}}{N}. \tag{45}$$

Again the sign of their difference determines which strategy parameters are chosen in the outer ES. Thus, we consider

$$R_+^{(g+1)} - R_-^{(g+1)} = \left( \frac{\sigma^{*2}}{2\beta\mu} - \frac{\beta\sigma^{*2}}{2\mu} \right) \frac{R^{(g)}}{N} = \left( \frac{1}{\beta} - \beta \right) \frac{\sigma^{*2}}{2\mu} \frac{R^{(g)}}{N}. \tag{46}$$

Because of the condition $\beta > 1$ this difference is always negative

$$R_+^{(g+1)} - R_-^{(g+1)} < 0. \tag{47}$$

That is, once the Meta-ES has reached its minimal isolation length $\gamma = 1$, the algorithm permanently increases the population size $\mu$ up to its maximum $\mu = d$ and maintains this state for the remaining isolation periods. This behavior has also been observed in Sec. 3, see Fig. 3.

# 5. INVESTIGATING THE MUTATION STRENGTH DYNAMICS

Due to the results of the iterated dynamics in Sec. 3 and our theoretical observations in Sec. 4, the $[1, 4(\mu, \lambda)^\gamma]$-Meta-ES is regarded to continuously increases the parental population $\mu$ to its maximal value $d = \mu\gamma$. As a consequence, the isolation length $\gamma$ reduces to 1 respectively. In this section we assume that the strategy has already reached its maximal population size and remains in this state according to Sec. 4.2. Therefore, we investigate the $\sigma$-dynamics regarding an $[1, 4(\mu, \lambda)^1]$-Meta-ES with $\beta = 1$. That is, neither the population size $\mu$ nor the isolation length $\gamma = 1$ will be changed by the outer ES. In the first step, Sec. 5.1 aims at a qualitative description of the $\sigma$ dynamics. This allows for an interpretation of the $\sigma$ dynamics observed in Sec. 3, Fig 4. Then in Sec. 5.2 we are going to investigate the dynamics of the normalized mutation strength. We provide a description of the $\sigma^*$ dynamics' asymptotic growth.

## 5.1 Explaining the $\sigma$-Dynamics

The outer ES generates two new $\sigma$-values from the parental mutation strength $\sigma^{(t)}$ ($t$ being the generation counter of the outer ES)

$$\sigma_+ := \alpha\sigma^{(t)} \quad \text{and} \quad \sigma_- := \sigma^{(t)}/\alpha. \tag{48}$$

Remembering Eq. (8), and writing $\sigma$ instead of $\sigma^{(t)}$, this results in two expected distances $R^{(t+1)}$ at the end of isolation period $t + 1$

$$R_+^{(t+1)} = R^{(t)} - \frac{\alpha\sigma c_{\mu/\mu,\lambda}}{\sqrt{1 + \frac{\sigma_\epsilon{}^2}{4R^{(t)2}\alpha^2\sigma^2}}} + \frac{\alpha^2\sigma^2 N}{2\mu R^{(t)}}, \tag{49}$$

$$R_-^{(t+1)} = R^{(t)} - \frac{\sigma c_{\mu/\mu,\lambda}}{\alpha\sqrt{1 + \frac{\alpha^2\sigma_\epsilon{}^2}{4R^{(t)2}\sigma^2}}} + \frac{\sigma^2 N}{2\alpha^2\mu R^{(t)}}. \tag{50}$$

Note that in contrast to Sec. 4, $R_+^{(t+1)}$ and $R_-^{(t+1)}$ now refer to the inner ES which operates with $\sigma_+$ and $\sigma_-$, respectively.
The algorithm chooses the parameters of the strategy which generates the smaller distance to the optimizer. That is, the sign of the difference $R_+^{(t+1)} - R_-^{(t+1)}$ determines whether the Meta-ES increases or decreases the mutation strength $\sigma$

$$\begin{aligned} R_+^{(t+1)} - R_-^{(t+1)} < 0 \quad &\Rightarrow \quad \sigma^{(t+1)} = \sigma^{(t)}\alpha \\ R_+^{(t+1)} - R_-^{(t+1)} > 0 \quad &\Rightarrow \quad \sigma^{(t+1)} = \sigma^{(t)}/\alpha. \end{aligned} \tag{51}$$

Combining (49) and (50), the difference $R_+^{(t+1)} - R_-^{(t+1)}$ reads

$$\frac{\alpha^2\sigma^2 N}{2\mu R^{(t)}} - \frac{\alpha\sigma c_{\mu/\mu,\lambda}}{\sqrt{1+\frac{{\sigma_\epsilon}^2}{4{R^{(t)}}^2\alpha^2\sigma^2}}} - \frac{\sigma^2 N}{2\alpha^2\mu R^{(t)}} + \frac{\sigma c_{\mu/\mu,\lambda}}{\alpha\sqrt{1+\frac{\alpha^2{\sigma_\epsilon}^2}{4{R^{(t)}}^2\sigma^2}}} \tag{52}$$

$$= \frac{\sigma^2 N}{2\mu R^{(t)}}\left(\alpha^2 - \frac{1}{\alpha^2}\right) - \left(\frac{\alpha\sigma c_{\mu/\mu,\lambda}}{\sqrt{1+\frac{{\sigma_\epsilon}^2}{4{R^{(t)}}^2\alpha^2\sigma^2}}} - \frac{\sigma c_{\mu/\mu,\lambda}}{\alpha\sqrt{1+\frac{\alpha^2{\sigma_\epsilon}^2}{4{R^{(t)}}^2\sigma^2}}}\right), \tag{53}$$

and considering the normalizations, see Eq. (5), it can be transformed into

$$\sigma\left[\frac{\sigma^*}{2\mu}\left(\alpha^2 - \frac{1}{\alpha^2}\right) - c_{\mu/\mu,\lambda}\left(\frac{\alpha}{\sqrt{1+\frac{\sigma_\epsilon^{*2}}{\alpha^2\sigma^{*2}}}} - \frac{1}{\alpha\sqrt{1+\frac{\alpha^2\sigma_\epsilon^{*2}}{\sigma^{*2}}}}\right)\right] \tag{54}$$

$$= \sigma\left[\frac{(\alpha^4-1)\sigma^*}{2\mu\alpha^2} - \frac{c_{\mu/\mu,\lambda}\sigma^*}{\alpha^2}\left(\frac{\alpha^4}{\sqrt{\alpha^2\sigma^{*2}+\sigma_\epsilon^{*2}}} - \frac{1}{\sqrt{\frac{\sigma^{*2}}{\alpha^2}+\sigma_\epsilon^{*2}}}\right)\right]. \tag{55}$$

Defining $\Delta$ by the term in the square brackets of Eq. (55)

$$\boxed{\Delta := \frac{(\alpha^4-1)\sigma^*}{2\mu\alpha^2} - \frac{c_{\mu/\mu,\lambda}\sigma^*}{\alpha^2}\left(\frac{\alpha^4}{\sqrt{\alpha^2\sigma^{*2}+\sigma_\epsilon^{*2}}} - \frac{1}{\sqrt{\frac{\sigma^{*2}}{\alpha^2}+\sigma_\epsilon^{*2}}}\right)} \tag{56}$$

the $\sigma$-dynamic depends only on the sign of $\Delta$, i.e.,

$$\begin{aligned} \Delta < 0 \quad &\Rightarrow \quad \sigma^{(t+1)} = \sigma^{(t)}\alpha, \\ \Delta > 0 \quad &\Rightarrow \quad \sigma^{(t+1)} = \sigma^{(t)}/\alpha. \end{aligned} \tag{57}$$

Note that $\Delta$ depends on the normalized mutation strength $\sigma^*$ as well as the normalized noise strength $\sigma_\epsilon^*$. With $\Delta(\sigma^*, \sigma_\epsilon^*)$ we have found the evolution equation for $\sigma$

$$\boxed{\sigma^{(t+1)} = \sigma^{(t)}\alpha^{-\mathrm{sign}(\Delta(\sigma^{*(t)},\sigma_\epsilon^{*(t)}))}.} \tag{58}$$

The sign of $\Delta$ is plotted depending on $\sigma^*$ and $\sigma_\epsilon^*$ in Fig. 6. The values of $\sigma^*$ and $\sigma_\epsilon^*$ are varied within their range of positive progress from zero to $2\mu c_{\mu/\mu,\lambda}$, see Eq. (6). Negative values of $\Delta(\sigma^*, \sigma_\epsilon^*)$ are represented by the yellow region, and positive ones by the red region respectively. For example, if the strategy operates with a combination of $\sigma^*$ and $\sigma_\epsilon^*$ values from the yellow region ($\Delta < 0$) it will increase the mutation strength after the isolation period.

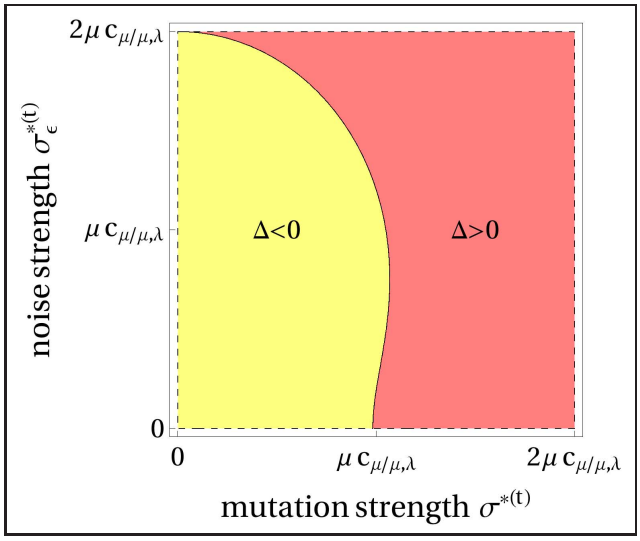


**Figure 6: On the sign of $\Delta$ depending on $\sigma^*$ and $\sigma_\epsilon^*$. The remaining parameters are $\mu = 256$, $\nu = 1/4$, and $\alpha = 1.2$**

We are interested in the critical value $\sigma_0^* > 0$ around which the sign of $\Delta(\sigma^*, \sigma_\epsilon^*)$ changes. According to the combination of $\sigma^*$ and $\sigma_\epsilon^*$ in Fig. 6 this critical value can be found on the black line between the two colored regions. Computing $\sigma_0^*$ from Eq. (56) leads directly to the condition

$$\frac{(\alpha^4-1)}{2\mu c_{\mu/\mu,\lambda}} \stackrel{!}{=} \frac{\alpha^4}{\sigma_\epsilon^*\sqrt{1+\frac{\alpha^2\sigma^{*2}}{\sigma_\epsilon^{*2}}}} - \frac{1}{\sigma_\epsilon^*\sqrt{1+\frac{\sigma^{*2}}{\alpha^2\sigma_\epsilon^{*2}}}}. \tag{59}$$

This must be solved for $\sigma^*$. Finding an analytical expression for $\sigma_0^*$ of (59) is demanding. Therefore, we apply the following approximation

$$\sqrt{1+\frac{\sigma^{*2}}{\sigma_\epsilon^{*2}}} \approx 1 + \frac{\sigma^{*2}}{2\sigma_\epsilon^{*2}}, \tag{60}$$

assuming that ${\sigma^{*2}}/{\sigma_\epsilon^{*2}} < 1$ holds when the Meta-ES has reached a certain vicinity to its steady state $\hat{R}_\infty$, see Eq. (12). Thus we can rewrite (59)

$$\frac{(\alpha^4-1)\sigma_\epsilon^*}{2\mu c_{\mu/\mu,\lambda}} \simeq \frac{\alpha^4}{1+\frac{\alpha^2\sigma^{*2}}{2\sigma_\epsilon^{*2}}} - \frac{1}{1+\frac{\sigma^{*2}}{2\alpha^2\sigma_\epsilon^{*2}}}. \tag{61}$$

Converting the fractions to a common denominator, we get

$$\frac{(\alpha^4-1)\sigma_\epsilon^*}{2\mu c_{\mu/\mu,\lambda}} \simeq \frac{(\alpha^4-1)}{1+\frac{\sigma^{*2}}{2\alpha^2\sigma_\epsilon^{*2}}+\frac{\alpha^2\sigma^{*2}}{2\sigma_\epsilon^{*2}}+\frac{\sigma^{*4}}{4\sigma_\epsilon^{*4}}}. \tag{62}$$

Rearranging the terms leads to

$$\frac{2\mu c_{\mu/\mu,\lambda}}{\sigma_\epsilon^*} \simeq 1 + \frac{\sigma^{*2}}{2\alpha^2\sigma_\epsilon^{*2}} + \frac{\alpha^2\sigma^{*2}}{2\sigma_\epsilon^{*2}} + \frac{\sigma^{*4}}{4\sigma_\epsilon^{*4}}, \tag{63}$$

and with further transformations we get a quadratic equation in $\sigma^{*2}$

$$\sigma^{*4} + 2\frac{\alpha^4+1}{\alpha^2}\sigma_\epsilon^{*2}\sigma^{*2} + 4\sigma_\epsilon^{*4}\left(1 - \frac{2\mu c_{\mu/\mu,\lambda}}{\sigma_\epsilon^*}\right) \simeq 0. \tag{64}$$

Solving (64) for $\sigma^{*2}$ yields

$$\sigma_0^{*2} \simeq -\frac{\alpha^4+1}{\alpha^2}\sigma_\epsilon^{*2} + \sqrt{\sigma_\epsilon^{*4}\left[\left(\frac{\alpha^4+1}{\alpha^2}\right)^2 + 4\left(\frac{2\mu c_{\mu/\mu,\lambda}}{\sigma_\epsilon^*} - 1\right)\right]}. \tag{65}$$

Taking the square root, one finally gets

$$\sigma_0^* \simeq \sigma_\epsilon^* \sqrt{\sqrt{\left(\frac{\alpha^4+1}{\alpha^2}\right)^2 + 4\left(\frac{2\mu c_{\mu/\mu,\lambda}}{\sigma_\epsilon^*} - 1\right)} - \left(\frac{\alpha^4+1}{\alpha^2}\right)}. \quad (66)$$

Dividing Eq. (66) by $\sigma_\epsilon^*$, one obtains

$$\frac{\sigma_0^*}{\sigma_\epsilon^*} \simeq \sqrt{\sqrt{\left(\frac{\alpha^4+1}{\alpha^2}\right)^2 + 4\left(\frac{2\mu c_{\mu/\mu,\lambda}}{\sigma_\epsilon^*} - 1\right)} - \left(\frac{\alpha^4+1}{\alpha^2}\right)}. \quad (67)$$

Note that for $\sigma_\epsilon = const.$, it holds

$$\sigma_\epsilon^* = \frac{\sigma_\epsilon N}{2R^2} \overset{R\to\hat{R}_\infty}{\longrightarrow} 2\mu c_{\mu/\mu,\lambda}. \quad (68)$$

Taking (68) into account, one sees that in (67) the critical value $\sigma_0^*$ in relation to the normalized noise strength $\sigma_\epsilon^*$ is decreasing to zero in the asymptotic limit. Figure 7 displays this behavior. A continuous increase of $\sigma_\epsilon^*$ to its maximal value $2\mu c_{\mu/\mu,\lambda}$ drives $\sigma_0^*/\sigma_\epsilon^*$ and $\sigma_0^*$ to zero.

Taking up the $\sigma_0^*$ behavior, we can continue with the qualitative analysis of the $\sigma$-dynamics. Equation (57) becomes

$$\begin{aligned} \sigma^* < \sigma_0^* \quad &\Rightarrow \quad \sigma^{(t+1)} = \sigma^{(t)}\alpha, \\ \sigma^* > \sigma_0^* \quad &\Rightarrow \quad \sigma^{(t+1)} = \sigma^{(t)}/\alpha. \end{aligned} \quad (69)$$

According to these equations, the Meta-ES adapts $\sigma$ so that the normalized mutation strength $\sigma^*$ reaches a certain vicinity to its point of discontinuity $\sigma_0^*$. In this region the $\sigma$ dynamics enter a limit cycle. This corresponds to the oscillatory behavior of the $\sigma$ dynamics which was already observed in Sec. 3, Fig. 4. The limit cycle will only be left if the point of discontinuity $\sigma_0^*$ changes. Notice that $\sigma_0^*$ still depends on the normalized noise strength $\sigma_\epsilon^*$. As long as the Meta-ES reduces the distance $R$ to the optimizer, $\sigma_\epsilon^*$ approaches its saturation value $2\mu c_{\mu/\mu,\lambda}$. Since the critical value $\sigma_0^*$ decreases

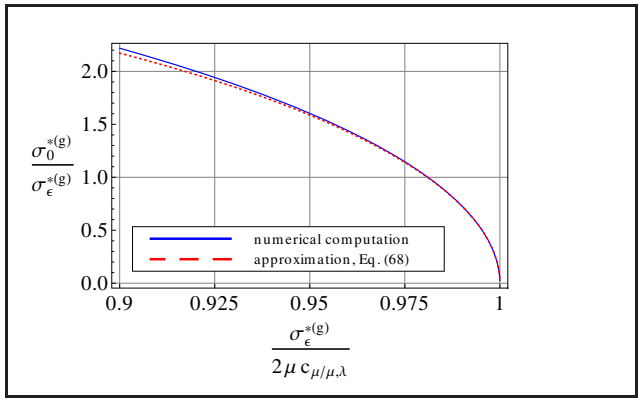


**Figure 7: The dashed red line shows the results of the approximation $\sigma_0^*/\sigma_\epsilon^*$, see Eq. (67). It is compared to the numerically computed root of Eq. (56) which is plotted with regard to $\sigma_\epsilon^*$ and represented by the solid blue line. The graph presents the results for $\sigma_\epsilon^*/2\mu c_{\mu/\mu,\lambda} \in [0.9, 1]$. One observes a good compliance between the numerical results and the approximation for $\sigma_\epsilon^*$ values in the vicinity of $2\mu c_{\mu/\mu,\lambda}$.**

tendentially, the strategy is able to leave the current $\sigma$ limit cycle and decrease the mutation strength until it enters the next limit cycle. This behavior explains the $\sigma$ dynamics in Sec. 3 where we observed a rather slow mutation strength decrease in stepwise limit cycles.

## 5.2 Calculating the $\sigma^*$-Dynamics

Now we consider the evolution of the normalized mutation strength $\sigma^*$ in order to analyze the steady state behavior of the Meta-ES. Remembering Eq. (5), Eq. (58), and taking into account

$$R^{(t+1)} = R^{(t)}\left(1 - \frac{1}{N}\varphi^*(\sigma^{*(t)}\alpha^{-\mathrm{sign}(\Delta(\sigma^{*(t)},\sigma_\epsilon^{*(t)}))}, \sigma_\epsilon^{*(t)})\right), \quad (70)$$

see Eq. (8), finally yields

$$\boxed{\sigma^{*(t+1)} = \sigma^{*(t)} \frac{\alpha^{-\mathrm{sign}(\Delta(\sigma^{*(t)},\sigma_\epsilon^{*(t)}))}}{1 - \frac{1}{N}\varphi^*(\sigma^{*(t)}\alpha^{-\mathrm{sign}(\Delta(\sigma^{*(t)},\sigma_\epsilon^{*(t)}))}, \sigma_\epsilon^{*(t)})}.} \quad (71)$$

Our goal is the computation of the expected normalized mutation strength dynamics $\sigma^*$ around which the ES oscillates in its steady state. At this point it should be noticed that the $\sigma^*$-dynamic directly interacts with the $\sigma_\epsilon^*$-dynamic. The latter determines the critical value $\sigma_0^*$ and thereby the strategy's behavior to increase or decrease the (normalized) mutation strength. That is, we have to solve an iterative mapping depending on $\sigma^{*(t)}$ and $\sigma_\epsilon^{*(t)}$

$$\sigma^{*(t+1)} = f_\sigma(\sigma^{*(t)}, \sigma_\epsilon^{*(t)}; \alpha, \mu, N). \quad (72)$$

With Eq. (5), and (8) we also derive the iterative mapping of the $\sigma_\epsilon^*$-dynamics

$$\boxed{\sigma_\epsilon^{*(t+1)} = \frac{\sigma_\epsilon^{*(t)}}{\left(1 - \frac{1}{N}\varphi^*(\sigma^{*(t)}\alpha^{-\mathrm{sign}(\Delta(\sigma^{*(t)},\sigma_\epsilon^{*(t)}))}, \sigma_\epsilon^{*(t)})\right)^2}.} \quad (73)$$

In order to calculate the asymptotic dynamics one has to apply various asymptotically exact simplifications. First, consider the progress rate

$$\varphi^*(\sigma^*, \sigma_\epsilon^*) = \frac{c_{\mu/\mu,\lambda}\sigma^{*2}}{\sqrt{\sigma_\epsilon^{*2} + \sigma^{*2}}} - \frac{\sigma^{*2}}{2\mu} \quad (74)$$

which asymptotically ($\sigma^*/\sigma_\epsilon^* \to 0$) can be expressed by

$$\varphi^*(\sigma^*, \sigma_\epsilon^*) = \frac{c_{\mu/\mu,\lambda}\sigma^{*2}}{\sigma_\epsilon^*\sqrt{1 + \frac{\sigma^{*2}}{\sigma_\epsilon^{*2}}}} - \frac{\sigma^{*2}}{2\mu} \quad (75)$$

$$\simeq \sigma^{*2}\left(\frac{c_{\mu/\mu,\lambda}}{\sigma_\epsilon^*} - \frac{1}{2\mu}\right) \quad (76)$$

$$= \underbrace{\frac{\sigma^{*2}}{2\mu\sigma_\epsilon^*}\left(2\mu c_{\mu/\mu,\lambda} - \sigma_\epsilon^*\right)}_{=:\,\tilde{\varphi}^*(\sigma^*,\sigma_\epsilon^*)}. \quad (77)$$

As a consequence one obtains a simpler $\sigma_\epsilon^*$-dynamics. Writing $\sigma^*$ and $\sigma_\epsilon^*$ instead of $\sigma^{*(t)}$ and $\sigma_\epsilon^{*(t)}$, it reads

$$\sigma_\epsilon^{*(t+1)} \simeq \frac{\sigma_\epsilon^*}{\left(1 - \frac{2}{N}\tilde{\varphi}^*(\sigma^*\alpha^{-\mathrm{sign}(\Delta(\sigma^*,\sigma_\epsilon^*))}, \sigma_\epsilon^*)\right)}. \quad (78)$$

Considering small progress in the asymptotic limit one can apply

$$\frac{1}{1-x} \approx 1 + x \quad \forall\, x \text{ with } |x| \ll 1 \quad (79)$$

resulting in

$$\sigma_\epsilon^{*(t+1)} \simeq \sigma_\epsilon^{*(t)}\left(1 + \frac{2}{N}\tilde{\varphi}^*(\sigma^{*(t)}\alpha^{-\mathrm{sign}(\Delta(\sigma^{*(t)},\sigma_\epsilon^{*(t)}))}, \sigma_\epsilon^{*(t)})\right). \quad (80)$$

Using $\tilde{\varphi}^*$, Eq. (77), one obtains

$$\sigma_\epsilon^{*(t+1)} \simeq \sigma_\epsilon^* + \frac{\sigma^{*2}\alpha^{-2\mathrm{sign}(\Delta(\sigma^*,\sigma_\epsilon^*))}}{\mu N}\left(2\mu c_{\mu/\mu,\lambda} - \sigma_\epsilon^*\right). \quad (81)$$

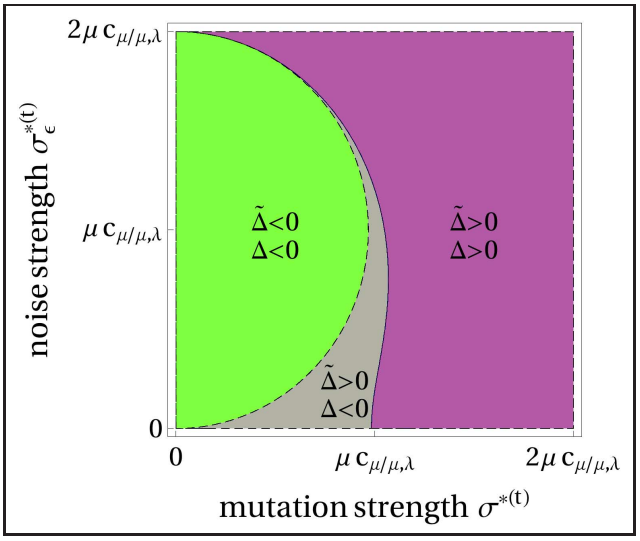


**Figure 8: Illustration of the trade-off between Δ, Eq. (56) and its approximation $\tilde{\Delta}$, Eq. (87).**

As a next step an approximation for $\Delta(\sigma^*, \sigma^*_\epsilon)$, Eq. (56) is needed. Assuming $\sigma^*/\sigma^*_\epsilon \to 0$, one finds the following asymptotical approximation

$$\frac{\sigma^*}{2\mu}\frac{\alpha^4-1}{\alpha^2} - \frac{\sigma^* c_{\mu/\mu,\lambda}}{\alpha^2 \sigma^*_\epsilon}\left(\frac{\alpha^4}{\left(1+\frac{\alpha^2\sigma^{*2}}{2\sigma^{*2}_\epsilon}\right)} - \frac{1}{\left(1+\frac{\sigma^{*2}}{2\alpha^2\sigma^{*2}_\epsilon}\right)}\right). \tag{82}$$

This can further be transformed into

$$\frac{\sigma^*}{\alpha^2}\left[\frac{(\alpha^4-1)}{2\mu} - \frac{c_{\mu/\mu,\lambda}}{\sigma^*_\epsilon}\left(\frac{(\alpha^4-1)}{1+\frac{\alpha^4+1}{\alpha^2}\frac{\sigma^{*2}}{2\sigma^{*2}_\epsilon}+\frac{\sigma^{*4}}{4\sigma^{*4}_\epsilon}}\right)\right] \tag{83}$$

$$= \frac{\sigma^*(\alpha^4-1)}{\alpha^2}\left(\frac{1}{2\mu} - \frac{4c_{\mu/\mu,\lambda}\sigma^{*3}_\epsilon}{4\sigma^{*4}_\epsilon + \sigma^{*4} + 2\frac{\alpha^4+1}{\alpha^2}\sigma^{*2}_\epsilon\sigma^{*2}}\right). \tag{84}$$

The term $\sigma^{*4}$ in the denominator of the subtrahend can be neglected considering small mutation strengths, i.e. $\sigma \to 0$. Thus, one obtains

$$\frac{\sigma^*(\alpha^4-1)}{\alpha^2}\left(\frac{1}{2\mu} - \frac{c_{\mu/\mu,\lambda}\sigma^*_\epsilon}{\sigma^{*2}_\epsilon + \frac{\alpha^4+1}{2\alpha^2}\sigma^{*2}}\right) \tag{85}$$

$$= \frac{\sigma^*(\alpha^4-1)}{2\mu\alpha^2\left(\sigma^{*2}_\epsilon + \frac{\alpha^4+1}{2\alpha^2}\sigma^{*2}\right)}\underbrace{\left(\sigma^{*2}_\epsilon + \frac{\alpha^4+1}{2\alpha^2}\sigma^{*2} - 2\mu c_{\mu/\mu,\lambda}\sigma^*_\epsilon\right)}_{=:\,\tilde{\Delta}(\sigma^*,\sigma^*_\epsilon)}. \tag{86}$$

The sign of Δ and, by implication, the decision inside the Meta-ES to increase or decrease the mutation strength $\sigma$ or $\sigma^*$, respectively, by the factor $\alpha$ is now only depending on

$$\boxed{\tilde{\Delta}(\sigma^*,\sigma^*_\epsilon) = \frac{\alpha^4+1}{2\alpha^2}\sigma^{*2} - \sigma^*_\epsilon\left(2\mu c_{\mu/\mu,\lambda} - \sigma^*_\epsilon\right).} \tag{87}$$

In Fig. 8 $\Delta(\sigma^*, \sigma^*_\epsilon)$, see Eq. (56), and its approximation $\tilde{\Delta}(\sigma^*, \sigma^*_\epsilon)$ are compared. The gray region ($\tilde{\Delta} > 0, \Delta < 0$) represents the trade-off between exact Δ and its approximation. Especially in the asymptotically interesting region of small $\sigma^*$ values and $\sigma^*_\epsilon \approx 2\mu c_{\mu/\mu,\lambda}$, the approximation shows a good agreement with Δ.
The results of the iterative computations of the original dynamics (71) and (73) lead to the conclusion that the $\sigma^*$-dynamics mainly depend on the $\alpha$ term. That is, the term $(1-\varphi^*/N)$ in (71) can be neglected and by combination with Eq. (87) this yields the following approximation of the $\sigma^*$-dynamics

$$\boxed{\sigma^{*(t+1)} = \sigma^{*(t)}\alpha^{-\mathrm{sign}(\tilde{\Delta}(\sigma^{*(t)},\sigma^{*(t)}_\epsilon))}.} \tag{88}$$

A conclusive asymptotic approximation of the $\sigma^*_\epsilon$-dynamics is found by inserting Eq. (87) into Eq. (81)

$$\boxed{\sigma^{*(t+1)}_\epsilon \simeq \sigma^{*(t)}_\epsilon + \frac{\left(\sigma^{*(t)}\alpha^{-\mathrm{sign}(\tilde{\Delta}(\sigma^{*(t)},\sigma^{*(t)}_\epsilon))}\right)^2}{\mu N}\left(2\mu c_{\mu/\mu,\lambda} - \sigma^{*(t)}_\epsilon\right).} \tag{89}$$

Note, if $\sigma^*$ is in the vicinity of $\sigma^*_0$, i.e. $\tilde{\Delta} \approx 0$, the analysis of the Meta-ES suggests an oscillatory behavior in the $\sigma^*$ values. Actually, such a behavior is observed, see Fig. 9. The actual $\sigma^*$ dynamics have a globally decreasing tendency superimposed by local oscillations. In Fig. 9 and Fig. 10 we validate the approximations (88) and (89) by comparing them with the original $\sigma^*$ and $\sigma^*_\epsilon$ dynamics from Eq. (71) and Eq. (73), respectively. The normalized noise strength is depicted in relation to its saturation value $2\mu c_{\mu/\mu,\lambda}$. Both dynamics are iterated over one million isolation periods of $\gamma = 1$ generation using a population size of $\mu = 10$ and a truncation ratio $\nu = 1/4$. The search space dimension is $N = 100$ and the adjustment parameter is set to $\alpha = 1.05$. The iterations start with $\sigma^*_\epsilon = 2\mu c_{\mu/\mu,\lambda} - 0.1$ and $\sigma^* = \sqrt{(2\mu c_{\mu/\mu,\lambda})^2 - \sigma^{*2}_\epsilon}$ to ensure the compliance with condition (6). In both figures the original dynamics are illustrated by solid blue lines while the dashed red lines represent the approximations. Notice the oscillating behavior of the normalized mutation strength dynamics in Fig. 9. With the continuous decrease of the difference $2\mu c_{\mu/\mu,\lambda} - \sigma^*_\epsilon$ in Fig. 10 also the critical value $\sigma^*_0$ slowly decreases, see Eq. (66). This way the $\sigma^*$ dynamics are able to leave their limit cycles from time to time which leads to the observable stepwise descent. Note that the phases of oscillation grow with decreasing $\sigma^*$. It can be observed that in both cases the slopes of the approximations and the original dynamics match after having evolved over a sufficiently large number of isolation periods. Therefore, one can use the approximation in order to compute the rate at which the mutation strength dynamics descent. To this end, combine the $\sigma^*$-, Eq. (88), and $\sigma^*_\epsilon$-dynamics from Eq. (89). Introduce the quantity $\delta^{(t)}$

$$\delta^{(t)} = 2\mu c_{\mu/\mu,\lambda} - \sigma^{*(t)}_\epsilon, \tag{90}$$

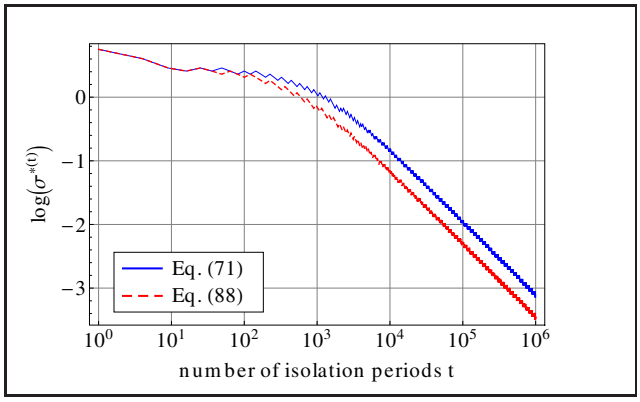


**Figure 9: The comparison of the iterated $\sigma^*$-dynamic from Eq. (71) represented by the blue line and its asymptotic approximation from Eq. (88) depicted as the red dashed line.**

that measures the deviation of the normalized noise strength $\sigma_\epsilon^*$ from its saturation value $2\mu c_{\mu/\mu,\lambda}$. Inserting (90) into (89), one obtains

$$\delta^{(t+1)} = \left(1 - \frac{\sigma^{*(t)^2}}{\mu N}\alpha^{-2\mathrm{sign}(\tilde{\Delta}(\sigma^{*(t)},\sigma_\epsilon^{*(t)}))}\right)\delta^{(t)}. \tag{91}$$

As one can see in Fig. 9, there are periods in the $\sigma^*$ evolution where the $\sigma^*$ values exhibits oscillatory behavior. This is reflected in the oscillatory change in the sign of $\tilde{\Delta}$. Since $\sigma_0^*$ corresponds to $\tilde{\Delta} = 0$ one has to mathematically treat the behavior at $\tilde{\Delta} = 0$, i.e. $\mathrm{sign}(\tilde{\Delta}) = \mathrm{sign}(0) = 0$. This immediately leads to (92).

$$\delta^{(t+1)} = \left(1 - \frac{\sigma^{*(t)^2}}{\mu N}\right)\delta^{(t)} \tag{92}$$

$$= \left(1 - \frac{\sigma^{*(t)^2}}{\mu N}\right)^{t+1}\delta^{(0)}. \tag{93}$$

With Eq. (93) we are able to simplify Eq. (87) in order to make a prediction about the asymptotic behavior of the $\sigma^*$-dynamics. In a first step Eq. (90) is inserted into (87) yielding

$$\tilde{\Delta}(\sigma^*, \delta^{(t)}) = \frac{\alpha^4+1}{2\alpha^2}\sigma^{*2} - 2\mu c_{\mu/\mu,\lambda}\delta^{(t)} + \delta^{(t)^2}. \tag{94}$$

Applying (93), the rhs becomes

$$\frac{\alpha^4+1}{2\alpha^2}\sigma^{*2} - 2\mu c_{\mu/\mu,\lambda}\left(1 - \frac{\sigma^{*2}}{\mu N}\right)^t\delta^{(0)} + \left(\left(1 - \frac{\sigma^{*2}}{\mu N}\right)^t\delta^{(0)}\right)^2 \tag{95}$$

$$= \frac{\alpha^4+1}{2\alpha^2}\sigma^{*2} - 2\mu c_{\mu/\mu,\lambda}\left(1 - \frac{\sigma^{*2}}{\mu N}\right)^t\delta^{(0)} + \left(1 - \frac{\sigma^{*2}}{\mu N}\right)^{2t}\delta^{(0)^2}. \tag{96}$$

Taking advantage of $\left(1 - \frac{\sigma^{*2}}{\mu N}\right)^t \simeq \left(1 - t\frac{\sigma^{*2}}{\mu N}\right)$ for $\frac{\sigma^{*2}}{\mu N} \ll 1$ one finds the asymptotical approximation of $\tilde{\Delta}(\sigma^*, \delta^{(0)})$

$$\frac{\alpha^4+1}{2\alpha^2}\sigma^{*2} - 2\mu c_{\mu/\mu,\lambda}\left(1 - t\frac{\sigma^{*2}}{\mu N}\right)\delta^{(0)} + \left(1 - 2t\frac{\sigma^{*2}}{\mu N}\right)\delta^{(0)^2}. \tag{97}$$

By further transformation one obtains

$$\left[\frac{\alpha^4+1}{2\alpha^2} + \left(\frac{2\delta^{(0)}(\mu c_{\mu/\mu,\lambda} - \delta^{(0)})}{\mu N}\right)t\right]\sigma^{*2} - 2\mu c_{\mu/\mu,\lambda}\delta^{(0)} + \delta^{(0)^2}. \tag{98}$$

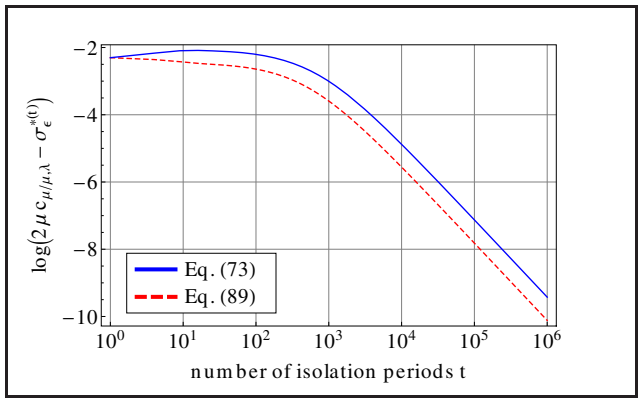


**Figure 10: The difference of the iterated $\sigma_\epsilon^*$-dynamic from Eq. (73) to the saturation value $2\mu c_{\mu/\mu,\lambda}$ (blue line) is compared to its asymptotic approximation given by the dynamics of Eq. (89), which are represented by the dashed red line.**

The root $\sigma_0^*$ of Eq. (98) can easily be found by solving $\tilde{\Delta} \stackrel{!}{=} 0$ resulting in

$$\sigma_0^* \simeq \sqrt{\frac{(2\mu c_{\mu/\mu,\lambda} - \delta^{(0)})\delta^{(0)}}{\frac{\alpha^4+1}{2\alpha^2} + \left(\frac{2\delta^{(0)}(\mu c_{\mu/\mu,\lambda} - \delta^{(0)})}{\mu N}\right)t}}. \tag{99}$$

That is, in the asymptotic limit the point of discontinuity $\sigma_0^*$ can be approximated by Eq. (99). The mutation strength dynamics oscillate around $\sigma_0^*$. Thus, we have found a description of the asymptotic $\sigma^*$-dynamics which only depends on the initial deviation $\delta^{(0)}$ of $\sigma_\epsilon^*$ from $2\mu c_{\mu/\mu,\lambda}$ and on the number of isolation periods $t$. In the next step we consider

$$\frac{(\alpha^4+1)}{2\alpha^2}\frac{1}{t} \stackrel{t\to\infty}{\longrightarrow} 0 \tag{100}$$

in order to develop an even simpler expression describing the asymptotic growth rate:

$$\boxed{\sigma_0^* \simeq \frac{\tau}{\sqrt{t}}.} \tag{101}$$

Here, we have substituted

$$\tau := \sqrt{\frac{\mu N(2\mu c_{\mu/\mu,\lambda} - \delta^{(0)})}{2\mu c_{\mu/\mu,\lambda} - 2\delta^{(0)}}}. \tag{102}$$

After a sufficiently large number of isolation periods, the descent of $\sigma_0^*$ is described by Eq. (101). It decreases obeying a square root law proportional to $\tau$. Since the $\sigma^*$ dynamics oscillate around $\sigma_0^*$ they consequently decrease with the same rate. That is, having evolved over a large number of isolation periods, the normalized mutation strength dynamics of the Meta-ES approach zero. In order to illustrate the compliance of this results we refer to the illustration in Fig. 11.

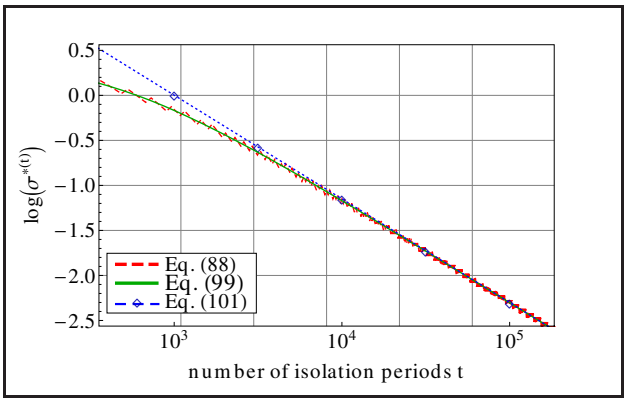


**Figure 11: Combination of the results from Fig. 9 with the prediction of Eq. (99) depicted by the solid green line which overlaps with the red dotted curve representing Eq. (88). The dashed blue line with markers represents the result of Eq. (101).**

The solid green line in Fig. 11 depicts the approximation of $\sigma_0^*$ from Eq. (99). Equation (101) is represented by the dashed blue line. One observes that the growth characteristics overlap in the asymptotic limit. It can be seen that the dashed red line, which asymptotically approximates the $\sigma^*$-dynamics, see Eq. (88), oscillates perfectly around the point of discontinuity $\sigma_0^*$.
At this point one can draw the following conclusion concerning the

asymptotic growth rate of the $\sigma$-dynamics. First note that the distance to the optimizer $R$ is nearly constant in the vicinity of the steady state distance $\hat{R}_\infty$. Considering $R \to \hat{R}_\infty$ and (5) one obtains

$$\sigma^* = \frac{N}{R}\sigma \simeq \sqrt{\frac{4\mu c_{\mu/\mu,\lambda} N}{\sigma_\epsilon}}\sigma. \tag{103}$$

Thus in the asymptotic limit the $\sigma$-dynamics exhibits a similar behavior as the $\sigma^*$-dynamics: The mutation strength oscillates around a critical value $\sigma_0$ which asymptotically decreases with $t$ according to

$$\boxed{\sigma_0 \simeq \frac{\tilde{\tau}}{\sqrt{t}}.} \tag{104}$$

Similar to $\sigma_0^*$, it decreases according to a square root law, however, with a different time constant $\tilde{\tau}$. The calculation of $\tilde{\tau}$ is beyond the scope of this paper.

## 6. SIMULATIONS

This section focuses on a comparison of the analytical investigations from the previous sections with the experimental runs of the $[1, 4(\mu/\mu_I, \lambda)^\gamma]$-Meta-ES algorithm presented in Sec. 2. This way we check the compliance of the results of the experiments with our theoretical predictions. The algorithm, see also Fig. 1 and Fig. 2, is initialized with parental population size $\mu_p = 2$ and truncation ratio $\nu = 1/4$ yielding $\lambda_p = 8$. The adjustment parameter of the population size is $\beta = 2$. We consider a search space dimensionality of $N = 1000$. The initial isolation time is set to $\gamma_p = 128$ which leads to an upper bound of $d = 256$ for the $\mu$ and $\gamma$ dynamics. The mutation strength is initialized at $\sigma_p = 1$ with adjustment parameter $\alpha = 1.05$. As the starting point of the algorithm we choose $(\mathbf{y_p})_i = 10$, $i = 1, \ldots, N$. This allows for a better observation of the point at which the influence of the constant fitness noise gains in importance. The noise strength is set to $\sigma_\epsilon = 5$. The algorithm is terminated after evolving over 10000 isolation periods.

The theoretical results are obtained by the iteration of Eq. (8) on the basis of the same initial values. The iteration proceeds as described at the end of Sec. 3. In the figures the results are displayed by the solid blue lines. Note that the iterated dynamics rely on the knowledge of the ideal fitness values in the selection process of the best inner ES. Whereas the selection in the experiments is based on the observed noisy fitness of the centroids returned by the inner strategies. This leads to deviations between iteratively generated and experimental results. In order to decrease the deviations we consider multiple experiments. Averaged over 20 independent runs of the algorithm the experimental results are presented as dashed red lines in Fig. 12 to Fig. 14.

Figure 12 depicts the $R$-dynamics of the Meta-ES. During the first 10 isolation periods the iterative and the experimental dynamics nearly match. Then the effects of the fitness noise can be observed. The iteratively computed $R$-dynamics approaches its expected residual steady state distance $\hat{R}_\infty$. The decrease of the experimentally obtained $R$ values decelerates. This results from the reduction of the isolation time $\gamma$, which is induced by increasing the population size. Regarding the population size dynamics in Fig. 13, we observe a good agreement provided that the strategy is able to increase the population size $\mu$. After having reached the maximal value $d = 256$, the corresponding isolation time is $\gamma = 1$. In this state the $\mu$-dynamics can either remain in its maximum or decrease again. Unlike our theoretical predictions suggest, the experimental $\mu$-dynamics leaves the state of maximal population size. Despite the population size fluctuates under the influence of noise, we can

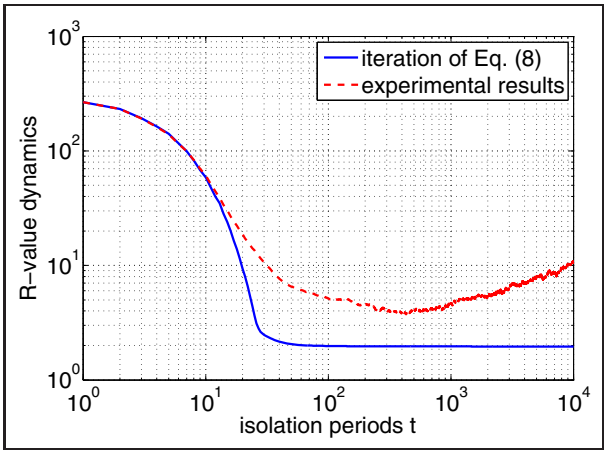


**Figure 12: Comparison of the distance to the optimizer, obtained by iteration of Eq. (8), with the results of the average of 20 independent experimental runs of the Meta-ES.**

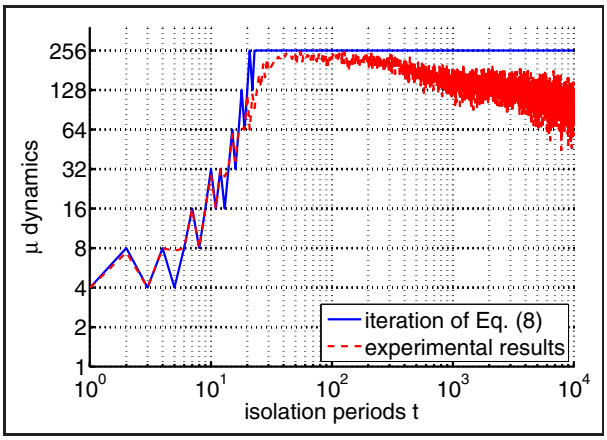


**Figure 13: The parental population size dynamics resulting from the experiment are depicted by the dashed red line. The iteratively computed dynamics resulting from Eq. (8) is represented by the solid blue line.**

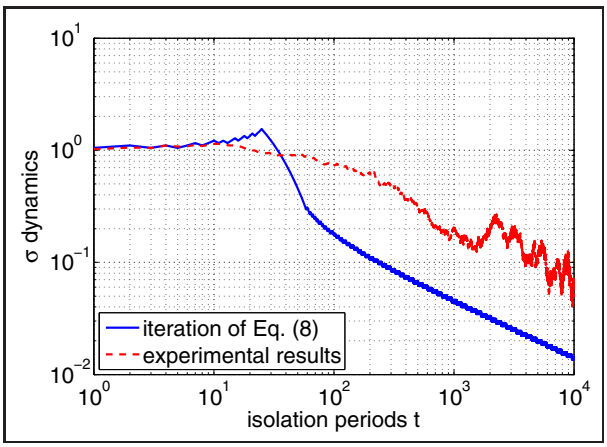


**Figure 14: The $\sigma$ dynamics resulting from Eq. (8) is compared to the experimental results. The mutation strength adjustment parameter is set to $\alpha = 1.05$.**

measure the strategy's tendency to favor greater population sizes. Considering the small isolation time and the influence of the fitness noise, we are able to explain the fluctuations. The smaller the fitness value the more it is affected by the noise. As the strategy approaches its residual steady state distance $\tilde{R}_\infty$ the noise disturbs the selection process. That is, the algorithm may select an inner strategy which decreases the population size, because it has the best observed noisy fitness. This leads the Meta-ES to leave its maximal population size $\mu = 256$ which directly influences the steady state distance $\tilde{R}_\infty$. Decreasing $\mu$ values cause $\tilde{R}_\infty$ to rise and consequently the $R$-dynamics increase, see Fig. 12. Since the population size is adjusted by the factor $\beta = 2$ this changes in the steady state distance can be relatively large. In Fig. 14 the $\sigma$-dynamics are displayed. Again one observes a good agreement of both dynamics during the first isolation periods.

At the point where the population size reaches its maximum the empirically generated results reveal significant deviations from the theoretical predictions. However, both dynamics show the same tendency to decrease the mutation strength $\sigma$. One can reduce the deviation by increasing the $\alpha$ factor, e.g. $\alpha = 1.2$. While this ensures a faster adaptation of the $\sigma$ values and thus getting closer to the theoretical $\sigma$ curve, the general deviation tendency does not change. The rather large deviations observed are due to the noisy fitness information which has not been included in the modeling of the selection process of the outer ES.

The theoretical analysis neglects the influence of fitness noise on the selection process of the outer ES. The dynamics resulting from the iteration of the theoretical equations rely on the knowledge of the expected ideal fitness values returned by the inner ESs. Whereas the selection in the experiments is based on the observed noisy fitness of the final parental centroids. This leads to significant deviations between theoretical and experimental dynamics. In order to confirm this explanation the following experiment has been conducted.

The real Meta-ES run can be emulated by adding noise to the fitness values of the theoretical predictions. In each isolation period a simulated noise term is added to the four iteratively generated fitness values resulting from the inner ESs. Selection within the iteration is then performed by choosing the best of these four "noisy" fitness values. The inner ES corresponding to the best observed fitness value provides its strategy parameters to the next iteration step. The noise term is modeled by a normally distributed random number with mean 0. Its variance is varying with the isolation period. For each isolation period this variance is determined by measuring the empirical variance of the four function values in the according isolation period of the real Meta-ES run. The empirical variances are averaged over 20 independent simulations. Also the iterative dynamics incorporating noise are averaged over 20 independent runs. Note, that the experimental dynamics are generated as explained in the beginning of this section. The initialization is maintained as well.

The iteration of Eq. (8) equipped with noise in the selection process of the outer ES is referred to as noisy iteration. The corresponding dynamics are illustrated by the solid blue lines in Fig. 15 to Fig. 17. The experimental dynamics are represented by dashed red lines.

Regarding the distance to the optimizer in this situation both dynamics fail to approach the minimal residual steady state distance $\hat{R}_\infty(d)$, see Fig. 15. $\hat{R}_\infty(d) = \sqrt{\frac{N\sigma_\epsilon}{4dc_{d/d,\lambda}}}$ corresponds to the maximal parental population size $\mu = d$ realizable by the Meta-ES algorithm.

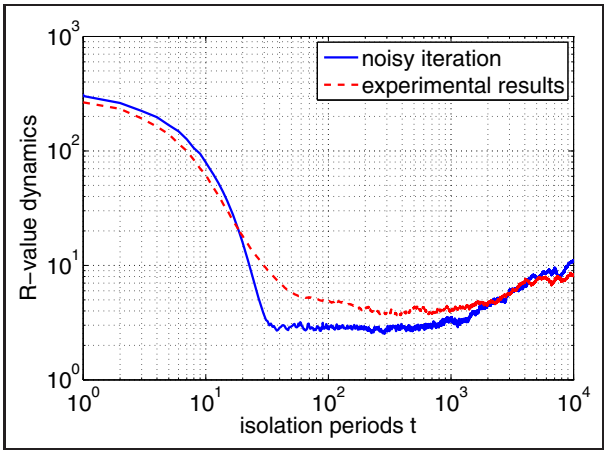


**Figure 15: Dynamics of the distance to the optimizer, obtained by iteration of Eq. (8) provided with noise, and the results of the experimental run of the Meta-ES.**

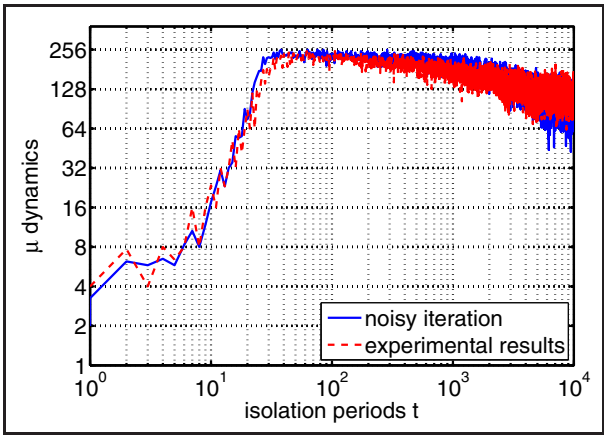


**Figure 16: The parental population size dynamics resulting from the experiment compared to the noisy iteration dynamics using Eq. (8).**

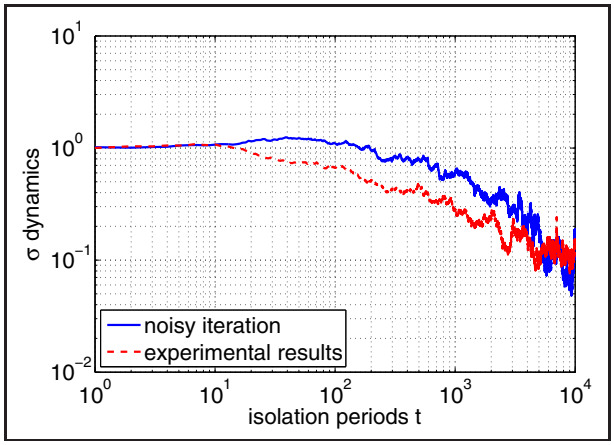


**Figure 17: The mutation strength dynamics resulting from Eq. (8) equipped with noise is compared to the experimental results.**

The deviations are a result of the fluctuations in the $\mu$ dynamics illustrated in Fig. 16. The noisy iteration as well as the experimental dynamics show larger deviations from the maximal parental population size $\mu = d$ with increasing number of isolation periods $t$. This behavior is resulting from the influence of fitness noise while selecting the best observed inner ES. Additionally, in Fig. 17 an improved agreement of the two mutation strength dynamics is observable.

In each case the iterative and the experimental dynamics show a similar behavior. Thus the behavior of the experimental dynamics can be reconstructed better by considering noise disturbances in the selection process of the theoretical model. This indicates that the deviations are - at least partially - a result of the disregard of selection noise in the theoretical modeling.

# 7. CONCLUSIONS AND OUTLOOK

In this paper we investigated the ability of a $[1, 4(\mu/\mu_I, \lambda)^\gamma]$-Meta-ES to simultaneously control the population size $\mu$ and the mutation strength $\sigma$ on the sphere model in particularly under the influence of fitness noise with constant variance. A theoretical analysis of the strategy's adaptation behavior has been presented. Considering asymptotically exact approximations we were able to calculate the general behavior of the $\mu$- as well as the $\sigma$-dynamics. While the $\mu$-dynamics increases $\mu$ exponentially fast up to the predefined $\mu$-bound, the $\sigma$-dynamics exhibits a square root law when approaching the steady state. That means that the approach to the steady state is rather slow.

The derivations presented assumed an error-free selection process in the meta strategy. In that point, the analysis deviates from the real Meta-ES. This deviation is the main reason for the deviations observed when comparing the theoretical results with real Meta-ES experiments.

One might consider to incorporate the noisy selection process of the outer ES in the analysis. This way the theoretical model would gain accuracy in reproducing the experimental dynamics. However, this is not really the direction of research we regard as a meaningful next step. The results rather indicate that the Meta-ES considered is not well suited for this noisy optimization problem. This leads to the question how to change the Meta-ES algorithmically such that it exhibits a better long-term behavior. That is, the selection process of the outer ES must be improved. One may think of various measures how to improve the selection process. For example, one could use $\gamma > 1$ runs to obtain more reliable fitness values (moving average). Investigations dealing with such questions will be next on our agenda.

# 8. ACKNOWLEDGMENTS

This work was supported by the Austrian Science Fund (FWF) under grant P22649-N23.

# 9. REFERENCES

[1] D. V. Arnold. *Noisy Optimization with Evolution Strategies.* Kluwer, 2002.

[2] D. V. Arnold and H.-G. Beyer. Local Performance of the $(\mu/\mu_I, \lambda)$-ES in a Noisy Environment. In *W. Martin and W. Spears, editors, Foundations of Genetic Algorithms, 6*, pages 127–141. Morgan Kaufmann, 2001.

[3] D. V. Arnold and A. MacLeod. Step length adaption on ridge functions. *Evolutionary Computation*, 16:151–184, 2008.

[4] H.-G. Beyer. *The Theory of Evolution Strategies*. Natural Computing Series, Springer, Heidelberg, 2001.

[5] H.-G. Beyer, M. Dobler, C. Hämmerle, and P. Masser. On Strategy Parameter Control by Meta-ES. GECCO-2009: Proceedings of the Genetic and Evolutionary Computation Conference, pages 499–506. ACM, 2009.

[6] H.-G. Beyer, M. Hellwig. Mutation Strength Control by Meta-ES on the Sharp Ridge. GECCO-2012: Proceedings of the Genetic and Evolutionary Computation Conference, pages 305–312. ACM, 2012.

[7] M. Herdy. Reproductive Isolation as Strategy Parameter in Hierarchically Organized Evolution Strategies. In *R. Männer and B. Manderick, editors, Parallel Problem Solving from Nature 2*, pages 207–217. Elsevier, 1992.

[8] I. Rechenberg. *Evolutionsstrategie '94*. Frommann-Holzboog Verlag, Stuttgart, 1994.